Verifying Multisensor Capacitive Resistivity Imaging (CRI) for Monitoring Rock-freezing Experiments

S.S. Uhlemann[1], O. Kuras[1], E.Haslam[1], P.I. Meldrum[1]

1 – British Geological Survey
suhl@bgs.ac.uk, oku@bgs.ac.uk, ehaslam@bgs.ac.uk, pime@bgs.ac.uk

Introduction

We have investigated and tested the applicability and limitations of a recently developed multi-sensor capacitive resistivity imaging (CRI) device for monitoring permafrost affected bedrock. CRI is a low-frequency EM measurement operating in a quasi-static mode, which emulates conventional electrical resistivity tomography (ERT) measurements without the need for galvanic coupling of the electrodes (Kuras et al. 2006). Temperature-calibrated ERT was shown to be capable of assessing the thermal state of permafrost and thus providing quantitative volumetric temperature information of permafrost (Krautblatter and Hauck 2007, Krautblatter et al. 2010). However, the high resistivities of frozen ground limit the applicability of galvanic sensors due to the resultant large range of contact resistances between sensors and the host material. A capacitively coupled system is expected to overcome these limitations, providing more robust data and higher-quality resistivity measurements within a temporal monitoring approach.

Numerical Simulations of Capacitive Resistivity Measurements

Finite-element forward modelling of CRI measurements was employed to validate the measurement concept of the prototype CRI system, and also to obtain an improved understanding of the physical processes taking place during the measurements. For this reason, we simulated CRI measurements for two situations: a homogeneous halfspace and a finite rock sample as used in laboratory experiments.

Within the homogeneous halfspace models we made a parameter study to investigate the effects of the geometric configuration of a capacitively coupled quadrupole. Accordingly, we changed sensor separation, sensor size, sensor elevation and halfspace resistivity. Figure 1 shows the key observations we obtained in this parameter study. For decreasing sensor separation and increasing sensor size, the discrepancy increases between the numerical simulation and an analytic model solution employing point poles. This reference solution justifies the use of conventional ERT methods to interpret the measured data (Kuras et al. 2006); hence, a large discrepancy implies limitations for the experimental array design. Therefore, dipole combinations with a separation smaller than twice the sensor size have to be avoided to stay below an anticipated measurement error of 5%. Sensor elevation and halfspace resistivity showed only minor effects on the transfer impedance.

We simulated the experimental array design to compare it with data measured on a rock sample in laboratory studies. 128 capacitive sensors were employed and 2408 dipole combinations simulated. By solving the model for different sample resistivities, it was shown that the simulated complex transfer impedances correlated with the sample resistivity, indicating the possibility to image changes in sample resistivity with the chosen configuration. Figure 2 shows the key observation for the simulation of CRI measurements on a finite rock sample. The complex signal was found to lie predominantly in the 4^{th} quadrant of the complex plane, i.e. in the experiments we had to expect positive real and negative imaginary parts. In accordance with theoretical estimations, the phase angle was very small (about 1°). An investigation of the potential distribution and current flow in the sample showed the broad and smooth coverage as would be expected for a galvanic DC measurement. Comparison with experimentally measured data showed reasonable agreement.

Laboratory Experiments on Tuffeau Chalk Sample

In order to examine the performance of the CRI method under different resistivity regimes, measurements were conducted during the course of a freeze-thaw cycle. A sample of Tuffeau chalk (0.3 m × 0.3 m × 0.45 m) was equipped with 128 capacitive and 32 galvanic resistivity sensors to measure apparent resistivities, 4 high-accuracy temperature sensors, and 2 TDR probes to assess the moisture content of the sample. The equipped

sample was placed in a thermally insulated, temperature regulated incubator to control its thermal state. The experimental configuration can be seen in Figure 3.

The sample temperature was gradually reduced from ~ 20˚C to -5˚C. CRI and ERT data were measured throughout this temperature range at certain steps, trying to ensure fairly constant temperature conditions of the sample within the measurement time (about 2 hours). Figure 4 shows the obtained average resistivity-temperature relationship during the freezing period. The behaviour of the resistivities with decreasing temperatures was as expected. Above the freezing point a linear increase with decreasing temperature was observed, whereas as soon as the temperatures decreased below the freezing point, resistivities increased very strongly following a quadratic shape. In this regime the resistivities followed the inverse of the volumetric water content, i.e. the ice content. Using the acquired data, a calibration curve was obtained to translate resistivities into temperatures. This curve was divided into two parts, a linear function above the freezing point and a quadratic function below. The offset between the CRI and ERT results in Figure 4 was found to be resistivity dependent and was thought to be an effect of certain experimental problems in the laboratory studies

Imaging Permafrost Processes with CRI

Permafrost processes are usually multi-scale and time variant, hence a technique trying to image these processes must be capable of resolving small changes in rock properties over multiple spatial scales and long time scales. To test the capabilities of the prototype CRI system, the measured data were not only interpreted in terms of their average values, but also resistivity inversion was applied to obtain 3D resistivity models of the sample at different temperatures. Figure 5 shows inverted data sets acquired at different sample temperatures. It shows that the CRI system is capable of imaging temperature-introduced changes in resistivity, while preserving sample specific properties. Changes in resistivity of about 400 Ωm could be imaged, resulting from temperature changes from 20˚C to -5˚C.

The calibration curve obtained previously was applied to these resistivity models and volumetric temperature models of the sample were obtained. Examples are shown in Figure 6. Above the freezing point temperature is not the dominating factor determining the resistivity; hence, the resistivity-based temperature estimate is not accurate. However, below the freezing point temperature dominates the resistivity response and the resistivity-based temperature models show very good agreement with the point estimates of the temperature probes. Therefore, assessing the thermal state of permafrost using measured resistivities is deemed reasonable.

Conclusions

We showed that multi-sensor CRI is suitable for investigating rock resistivities during the course of freezing experiments. The newly developed system was proven to be capable of resolving changes in resistivity due to changes in temperature. Assessing the thermal state of permafrost by measured resistivities showed good agreement with measured point data. Numerical simulations validated the measurement principle and revealed limitations on the experimental array design.

Acknowledgement

Our work is funded by a Natural Environment Research Council (NERC) Technology Proof of Concept grant award (NE/I000917/1). This paper is published with the permission of the Executive Director of the British Geological Survey (NERC).

References

Krautblatter, M. and Hauck, C. [2007] Electrical resistivity tomography monitoring of permafrost in solid rock walls. *Journal of Geophysical Research*, **112**(F2), 1-14.

Krautblatter, M., Verleysdonk, S., Flores-Orozco, A. and Kemna, A. [2010] Temperature-calibrated imaging of seasonal changes in permafrost rock walls by quantitative electrical resistivity tomography (Zugspitze, German/Austrian Alps). *Journal of Geophysical Research*, **115**(F2), 1-15.

Kuras, O., Beamish, D. and Meldrum, P. [2006] Fundamentals of the capacitive resistivity technique, *Geophysics*, **71**(3), G135-G152.

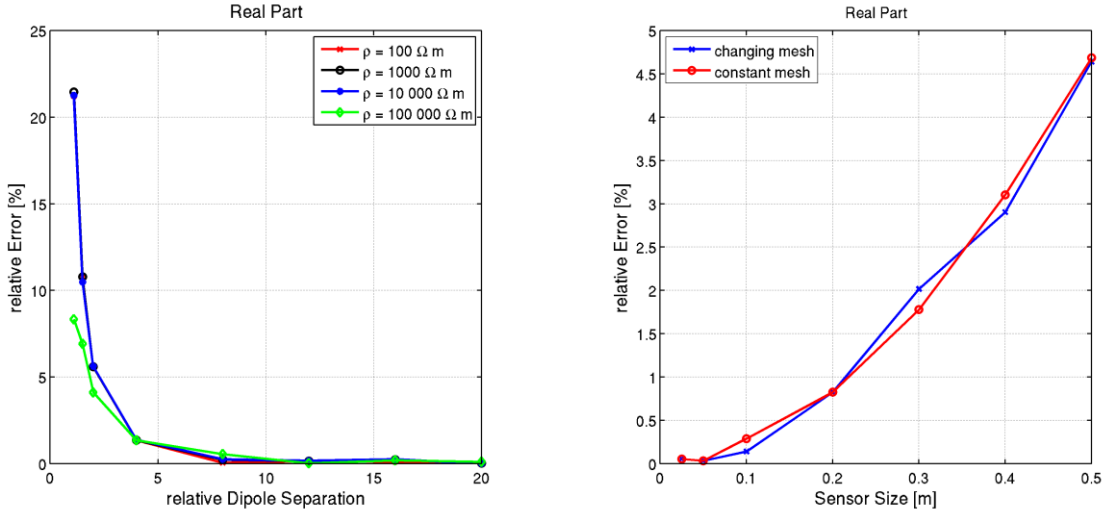

Figure 1 Differences between simulated and analytically derived complex transfer impedances for different sensor separations (left) and sensor sizes (right). Large errors imply violation of the point-pole approximation of the analytic solution and hence show effects of the finite size of the capacitive sensors.

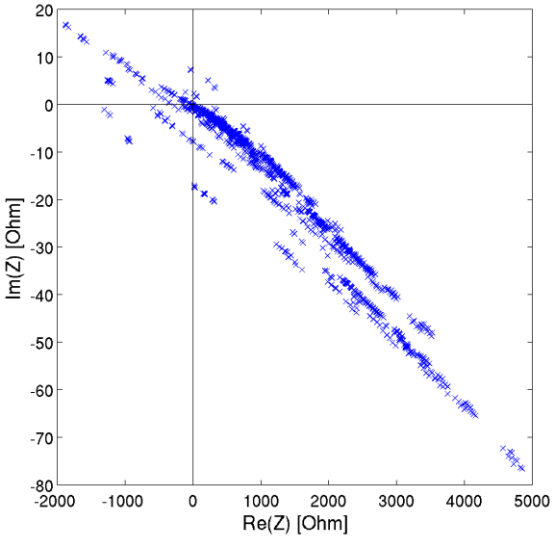

Figure 2 Simulated complex transfer impedance for 2408 different dipole combinations. The majority of data points lie in 4th quadrant of the complex plane (i.e. positive real and negative imaginary part). Note the different scales of the axes.

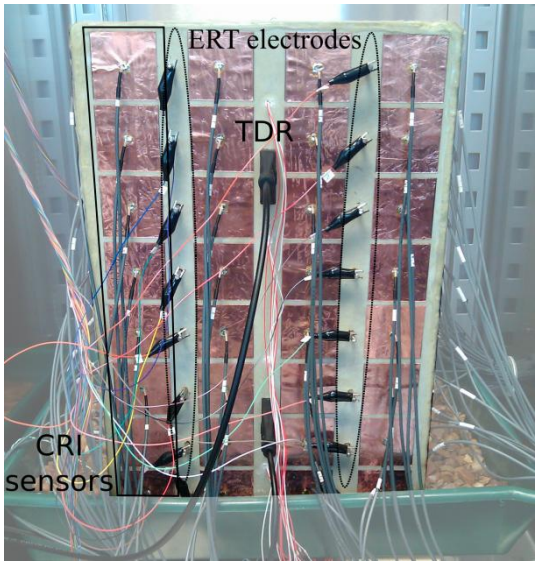

Figure 3 Experimental setup of different sensors and probes employed in the laboratory studies. CRI sensors are made of copper foil arranged in a regular grid over the sample faces. ERT electrodes are distributed in 2 lines with 8 electrodes each on two opposite faces of the sample. Moreover, the sample was equipped with 2 TDR and 4 temperature probes to monitor the moisture content and thermal state.

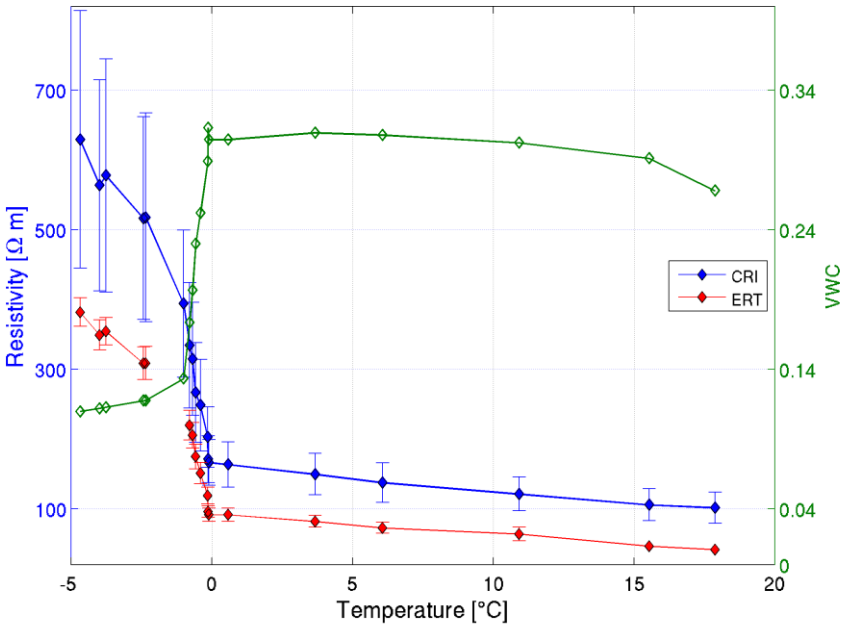

Figure 4 Resistivity-temperature relationship. Resistivity data are mean values of corresponding data sets. CRI and ERT show a very similar behaviour. The offset between them is expected to result from certain experimental problems.

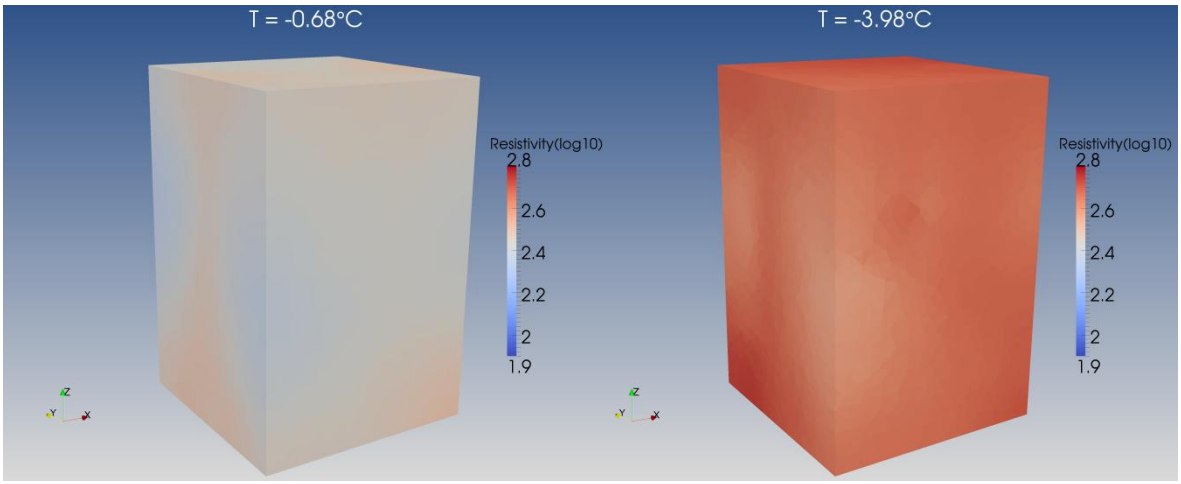

Figure 5 Inverted resistivity models from CRI data sets acquired at different temperatures. Lower temperature is clearly related to higher resistivity. The two results show the dependency of the sample resistivity on temperature, but also show that sample specific structures are preserved.

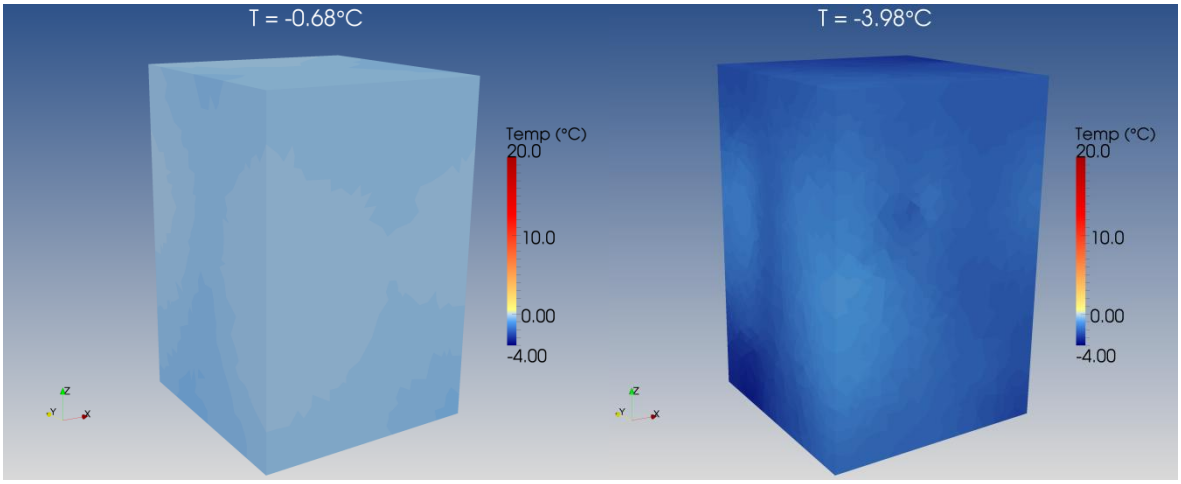

Figure 6 Resistivity-based volumetric temperature models, derived from applying calibration curve on the resistivity models shown in Figure 5. The different temperatures can be distinguished and are in good accordance with the point measurements (indicated above the models).